RHAMM^B-mediated bifunctional nanotherapy targeting Bcl-xL and mitochondria for pancreatic neuroendocrine tumor treatment

Xiang Chen,[1,5] Seung Koo Lee,[2,5] Mei Song,[3] Tiantian Zhang,[1] Myung Shin Han,[2] Yao-Tseng Chen,[1] Zhengming Chen,[4] Xiaojing Ma,[3] Ching-Hsuan Tung,[2] and Yi-Chieh Nancy Du[1]

[1]Department of Pathology and Laboratory Medicine, Weill Cornell Medicine, New York, NY 10065, USA; [2]Molecular Imaging Innovations Institute, Department of Radiology, Weill Cornell Medicine, New York, NY 10065, USA; [3]Department of Microbiology and Immunology, Weill Cornell Medicine, New York, NY 10065, USA; [4]Division of Biostatistics and Epidemiology, Department of Population Health Sciences, Weill Cornell Medicine, New York, NY 10065, USA

The incidence of pancreatic neuroendocrine tumor (PNET) has continued to rise. Due to their indolent feature, PNET patients often present with incurable, metastatic diseases. Novel therapies are urgently needed. We have previously shown that Receptor for Hyaluronic Acid-Mediated Motility isoform B (RHAMM^B) and Bcl-xL are upregulated in PNETs and both of them promote PNET metastasis. Because RHAMM protein is undetectable in most adult tissues, we hypothesized that RHAMM^B could be a gateway for nanomedicine delivery into PNETs. To test this, we developed a RHAMM^B-targeting nanoparticle (NP). Inside this NP, we assembled small interfering RNA (siRNA) against Bcl-xL (siBcl-xL) and mitochondria-fusing peptide KLA. We demonstrated that RHAMM^B-positive PNETs picked up the RHAMM^B-targeting NPs. siBcl-xL or KLA alone killed only 30% of PNET cells. In contrast, a synergistic killing effect was achieved with the co-delivery of siBcl-xL and KLA peptide in vitro. Unexpectedly, siBcl-xL induced cell death before reducing Bcl-xL protein levels. The systemically injected RHAMM^B-targeting NPs carrying siBcl-xL and KLA peptide significantly reduced tumor burden in mice bearing RHAMM^B-positive PNETs. Together, these findings indicate that the RHAMM^B-targeting nanotherapy serves as a promising drug delivery system for PNET and possibly other malignancies with upregulated RHAMM^B. The combination of siBcl-xL and KLA peptide can be a therapy for PNET treatment.

INTRODUCTION

Pancreatic neuroendocrine tumors (PNETs) represent one-third of gastroenteropancreatic neuroendocrine tumors and are the second most common malignancy of the pancreas.[1,2] The incidence of PNETs have continued to rise.[3] Due to their indolent feature, PNET patients often present with incurable, metastatic diseases. The 5-year survival rate of metastatic PNETs is only about 15%.[4] Sunitinib (a multi-targeted protein tyrosine kinase inhibitor) and everolimus (an mTOR inhibitor) are used for the treatment of unresectable and progressive or metastatic PNETs.[5,6] However, both of them only extend the median patient survival by approximately 6 months, and all patients eventu-

ally develop drug resistance.[6] Therefore, a better treatment strategy is vitally needed to improve clinical outcome.

Because evading apoptosis is a hallmark of cancer,[7] restoration of the apoptotic pathway in cancer has been an area of active research. Previous studies have demonstrated that a KLA peptide with a sequence of (KLAKLAK)$_2$ can induce apoptosis in cancer cells.[8] This group of peptides facilitates apoptosis via disrupting the mitochondrial outer membrane. Moreover, anti-apoptotic Bcl-xL (BCL2L1) family proteins have been investigated as therapeutic targets.[9] The upregulation of the Bcl-xL family members is one of the defining features of cancer cells in comparison to normal cells, and significantly contributes to chemoresistance and radioresistance.[10–12] Small molecule inhibitors of Bcl-xL were thus proposed as drugs; however, the clinical trials found unsatisfactory anti-tumor effect and patients experienced thrombocytopenia because Bcl-xL is essential for the longevity of platelets.[13,14] In addition to its well-known anti-apoptotic function, we discovered that the overexpressed Bcl-xL in PNETs promotes metastasis independent of its canonical anti-apoptotic activity.[15] The dual functions of Bcl-xL in anti-apoptosis and metastasis make it an attractive therapeutic target in metastatic PNETs. We hypothesized that a method to bring this pro-apoptotic pair, small interfering RNA (siRNA) against Bcl-xL and mitochondria-fusing peptide KLA, to PNETs may synergize the anti-cancer effect.

Receptor for Hyaluronic Acid-Mediated Motility (RHAMM or HMMR) was identified as a protein that binds to hyaluronic acid (HA).[16] RHAMM has limited protein expression in adult human tissues, but it is upregulated in histologically high-grade tumors in general.[17] Several RHAMM alternative splicing isoforms have been
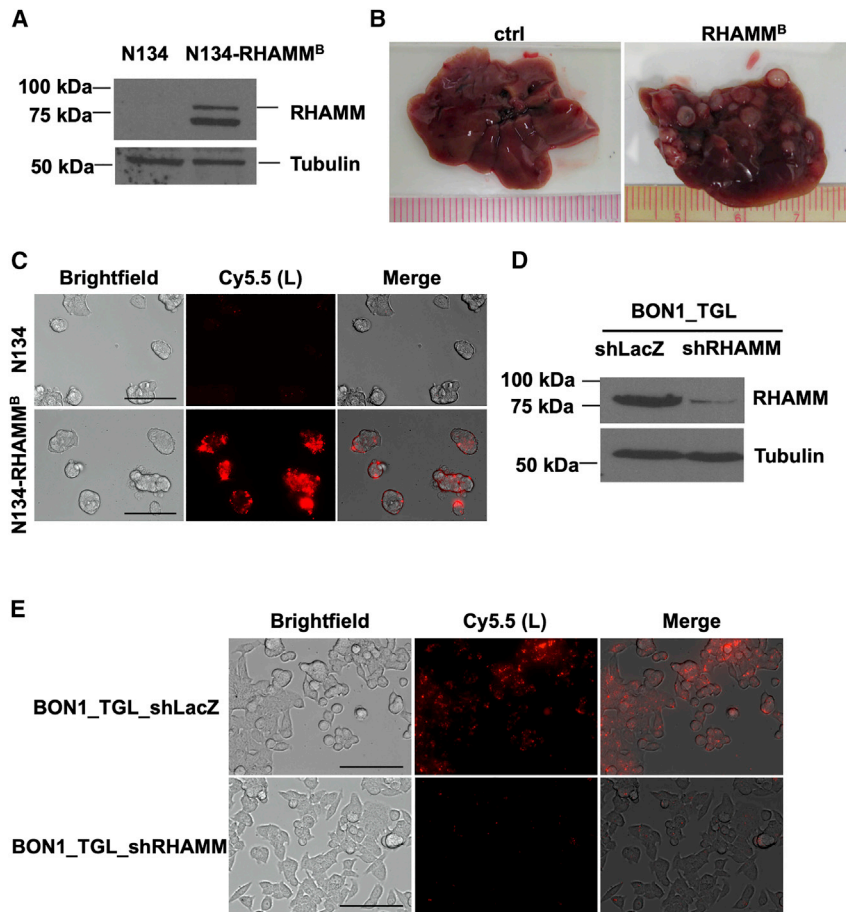
Figure 1. RHAMM[B] is crucial for liver metastasis of PNET cells and mediates cellular uptake of RHAMM[B]-targeting HA-coated NPs (Au/L/HA)

(A) Western blot analysis of human RHAMM in mouse PNET N134 and N134-RHAMM[B] cells. (B) Representative liver photos from mice injected with N134 and N134-RHAMM[B] cells at the end point. 2×10^6 N134 or N134-RHAMM[B] cells were injected into NSG mice (n = 5) through the tail vein. 6 weeks later, mice were euthanized to survey for metastatic sites and incidence. (C) Target-specific uptake of Au/L/HA (0.08 nmol) in N134-RHAMM[B] cells compared to N134 cells (magnification: ×40). Scale bar, 100 μm. (D) Western blot analysis of human RHAMM in human PNET BON1_TGL_shLacZ and BON1_TGL_shRHAMM cells. (E) Specific uptake of Au/L/HA in BON1_TGL_shLacZ cells compared to BON1_TGL_shRHAMM (magnification: ×40). Scale bar, 100 μm. Au, gold NP; L, PLL-Cy5.5.

identified, and we have previously found that RHAMM isoform B (RHAMM[B]) was the predominant isoform upregulated in human PNETs and various cancers.[17–20] We have previously demonstrated the metastatic function of human RHAMM *in vitro* and *in vivo*. Overexpression of RHAMM[B] significantly promotes metastasis of mouse and human PNETs in spontaneous and experimental metastasis mouse models.[21] Knockdown of RHAMM reduced migration of human lung cancer cell lines and liver metastasis of human PNET in mouse model.[18,20] We hypothesized that RHAMM[B]-targeting delivery may target PNETs specifically with minimal adverse effects to other cells. In this study, we aim to develop gold nanoparticles (AuNPs) carrying siBcl-xL and KLA peptide to specifically target RHAMM[B]-overexpressing PNETs. AuNP-based delivery system was selected as the delivery vehicle for this RHAMM-targeting combination therapy based on the favorable properties of AuNPs, including tunable size, surface modification, biocompatibility, low cytotoxicity,[23] and our prior experiences.[24]

RESULTS

RHAMM[B] is crucial in PNETs and mediates cellular uptake of HA-coated AuNPs in PNET cells

To validate the critical role of human RHAMM[B] in metastatic progression of PNETs,[18] we generated a new batch of mouse PNET N134 cells

expressing human RHAMM[B]. The expression of human RHAMM[B] (~82 kDa) was verified in the new N134-RHAMM[B] cell line by western blotting using an antibody specific against human RHAMM (Figure 1A). An additional lower molecular weight band was detected only in N134-RHAMM[B] cells, likely representing a degradation product of RHAMM protein. To confirm the metastatic function of RHAMM[B] *in vivo*, we injected 2×10^6 N134 or N134-RHAMM[B] cells into immunodeficient non-obese diabetic/severe combined immunodeficiency interleukin-2Rgc (NOD/SCID-IL2Rgc) knockout (NSG) mice via tail vein (n = 5). 6 weeks later, we euthanized the recipient mice. None of the mice receiving N134 cells developed liver metastases and all 5 mice receiving N134-RHAMM[B] cells developed large liver metastases (Figure 1B), supporting the metastatic function of human RHAMM[B].

RHAMM is a receptor of HA. To investigate the potential of HA-coated AuNPs to specifically target human RHAMM[B]-expressing mouse PNET cells, we prepared Au/L/HA NPs (Table 1). AuNPs was first layered by positively charged poly-L-lysine (PLL) and then coated with negatively charged HA on the surface of NPs. For tracking purposes, PLL were labeled by Cy5.5. We added Au/L/HA NPs into the culture medium of N134 and N134-RHAMM[B] cells. 12 h later, we observed a strong intracellular Cy5.5 fluorescence signal in N134-RHAMM[B] cells, but no signals in N134 cells, suggesting that HA-coated AuNPs were selectively picked up by RHAMM[B]-expressing PNET cells (Figure 1C). To further verify the RHAMM[B]-dependent HA-coated AuNPs uptake, we used a previously generated human PNET cell line with reduced level of RHAMM by short hairpin RNA (shRNA) knockdown (BON1_TGL_shRHAMM) and a control cell line (BON1_TGL_shLacZ; Figure 1D).[18] We have reported that BON1 cells upregulate RHAMM, especially RHAMM[B] isoform, compared to normal human islets.[18] We incubated

Table 1. Various nanocomplexes generated in this study

	Layer 1 (+)	Layer 2 (−)	Layer 3 (+)	Layer 4 (−)
Au/K	KLA[a]			
Au/L/HA	PLL[a]	HA		
Au/L/siB/L	PLL[a]	Bcl-xL siRNA	PLL	
Au/L/siC/L	PLL[a]	Scramble control siRNA	PLL	
Au/L/siB/K	PLL[a]	Bcl-xL siRNA	KLA[a]	
Au/L/siB/K/HA	PLL[a]	Bcl-xL siRNA	KLA[a]	HA

[a]For tracking purpose, KLA and PLL were labeled by FITC and Cy5.5, respectively.

BON1_TGL_shLacZ and BON1_TGL_shRHAMM cells with Au/L/HA NPs for 12 h and then imaged the cells under a fluorescence microscope. BON1_TGL_shRHAMM cells showed significantly decreased cellular uptake of HA-coated AuNPs compared with BON1_TGL_shLacZ cells (Figure 1E).

RHAMM and Cluster of Differentiation 44 (CD44) are two major receptors of HA.[25] To address whether CD44 may also facilitate the uptake of HA-coated AuNPs in N134-RHAMM[B] cells, we determined the CD44 expression levels in N134 and N134-RHAMM[B] cells. We stained CD44 on the surface of N134 and N134-RHAMM[B] cells using Alexa Fluor 488 conjugated anti-CD44 antibody followed by live cell imaging. We found that CD44 was not detectable on the cell surface of both N134 and N134-RHAMM[B] cells (Figure S1). MCF7 cell line, which had low CD44 expression, and MDA-MB-231 cell line with high endogenous CD44 expression were used as negative and positive controls (Figure S1).[26] Taken together, the expression of RHAMM[B] without CD44 on the cell surface was sufficient for the cellular uptake of HA-coated AuNPs by RHAMM[B]-expressing PNET cells.

Development of RHAMM[B]-targeting nanotherapy carrying siRNA against Bcl-xL and KLA peptide

We previously demonstrated that Bcl-xL promoted PNET metastasis independent of its anti-apoptosis function.[15] The dual functions of Bcl-xL in anti-apoptosis and metastasis make it an attractive therapeutic target in metastatic PNETs. We utilized the layer-by-layer fabrication strategy[27] to assemble siRNA against Bcl-xL (siBcl-xL) inside the HA-coated AuNPs (Table 1). We sequentially layered the negatively charged AuNP core with PLL-Cy5.5 (+), siBcl-xL (−), PLL (+), and HA (−) using charge-charge interactions (Figure S2). To determine the functional efficacy of the HA-coated AuNPs carrying siBcl-xL (siB), we incubated N134-RHAMM[B] cells with Au/L/HA, Au/L/ scramble control siRNA (siC)/L/HA, Au/L/siBcl-xL(siB)/L/HA in the cell culture medium for 12 h. Then, NP-containing medium was replaced with regular medium (Figure 2A). Cell viability of N134-RHAMM[B] cells incubated with Au/L/siB/HA was reduced at 48 h and 72 h (Figure 2B). Detection of activated caspase-3 offers an easy, sensitive, and reliable method for detecting and quantifying apoptosis. Caspase-3 activity in N134-RHAMM[B] cells incubated with Au/L/siB/L/HA was also observed at 48 h and 72 h, but not in untreated cells or cells treated with Au/L/HA and Au/L/siC/L/HA (Fig-

ure 2C; Figure S3). The reduction of Bcl-xL protein levels was observed at 72 h in N134-RHAMM[B] cells incubated with Au/L/siB/HA, but not in untreated cells or cells treated with Au/L/HA and Au/L/siC/L/HA (Figure 2D). This suggested that siBcl-xL in the HA-coated AuNP knocked down Bcl-xL expression. Surprisingly, the reduction of Bcl-xL protein levels was not obvious at 48 h in N134-RHAMM[B] cells incubated with Au/L/siB/HA (Figure 2D), when caspase-3 activity was elevated and ∼30% of cells lost their viability (Figures 2B and 2C). The data suggested that siBcl-xL has a novel way to induce cell death before downregulating Bcl-xL protein expression.

To increase the cytotoxicity of the HA-coated AuNPs, we co-delivered siBcl-xL with a KLA mitochondria-fusing peptide. KLA is an amphipathic antimicrobial peptide.[8] Although KLA can disrupt bacterial cell membrane, it cannot penetrate eukaryotic plasma membrane. However, once inside eukaryotic cells, it can disrupt the mitochondrial membrane and cause apoptosis.[28] We hypothesized that the co-delivery of siBcl-xL and KLA peptide will synergize to drive apoptosis. To generate RHAMM[B]-targeting AuNPs co-delivering siBcl-xL and KLA peptides, we sequentially layered the negatively charged AuNP core with PLL-Cy5.5 (+), siBcl-xL (−), KLA-fluorescein isothiocyanate (FITC; +), and HA (−) using charge-charge interactions (Figure 3A). To track the nanocomplexes in vitro and in vivo, we conjugated PLL and KLA with Cy5.5 and FITC fluorescence, respectively. For the characterization of RHAMM[B]-targeting nanocomplexes, we measured the size of the nanocomplexes by dynamic light scattering (DLS) after each layer of coating. As shown in Figure 3B, the size of the initial bare AuNP was 40 nm and its size increased steadily with the number of layers added. Au/L: 75 nm; Au/L/siBcl-xL (Au/L/siB): 88 nm; Au/L/siBcl-xL/KLA (Au/L/siB/K): 98 nm; Au/L/siBcl-xL/ KLA/HA (Au/L/siB/K/HA): 112 nm.

To confirm the success of each coating by charge-charge interactions, we measured the zeta potential,[29] which is the net surface charge of the NP (Figure 3B). The initial zeta potential of bare AuNPs was −31 mV. The PLL coating brought the surface charge up to about +34 mV. The subsequent siRNA layer dragged it down to about −26 mV and the KLA layer converted it to +24 mV. The final surface charge of the assembled Au/L/siB/K/HA was about −30 mV. The zigzag pattern of the surface zeta potential demonstrated the successful coating of each layer (Figure 3B). The prepared Au/L/siB/K/HA NPs were stable and the particle size was not changed up to 2 days in serum containing medium (Figure S4).

To examine cellular uptake and cytotoxicity of nanocomplexes, we treated N134 or N134-RHAMM[B] cells with various NPs including Au/L/siC/L, Au/L/siB/L, Au/K, Au/L/siB/K, Au/L/HA, and Au/L/ siB/K/HA for 12 h. After additional culture for 48 h, we examined the internalization of FITC-conjugated KLA peptide and Cy5.5-conjugated PLL under a fluorescent microscope. The untreated N134 and N134-RHAMM[B] cells were used as controls. As expected, the negatively charged Au/L/siB/K/HA could not be internalized by N134 cell. No fluorescent signal was detected due to the lack of HA-RHAMM binding in RHAMM[B]-negative N134 cells (Figure 4A).
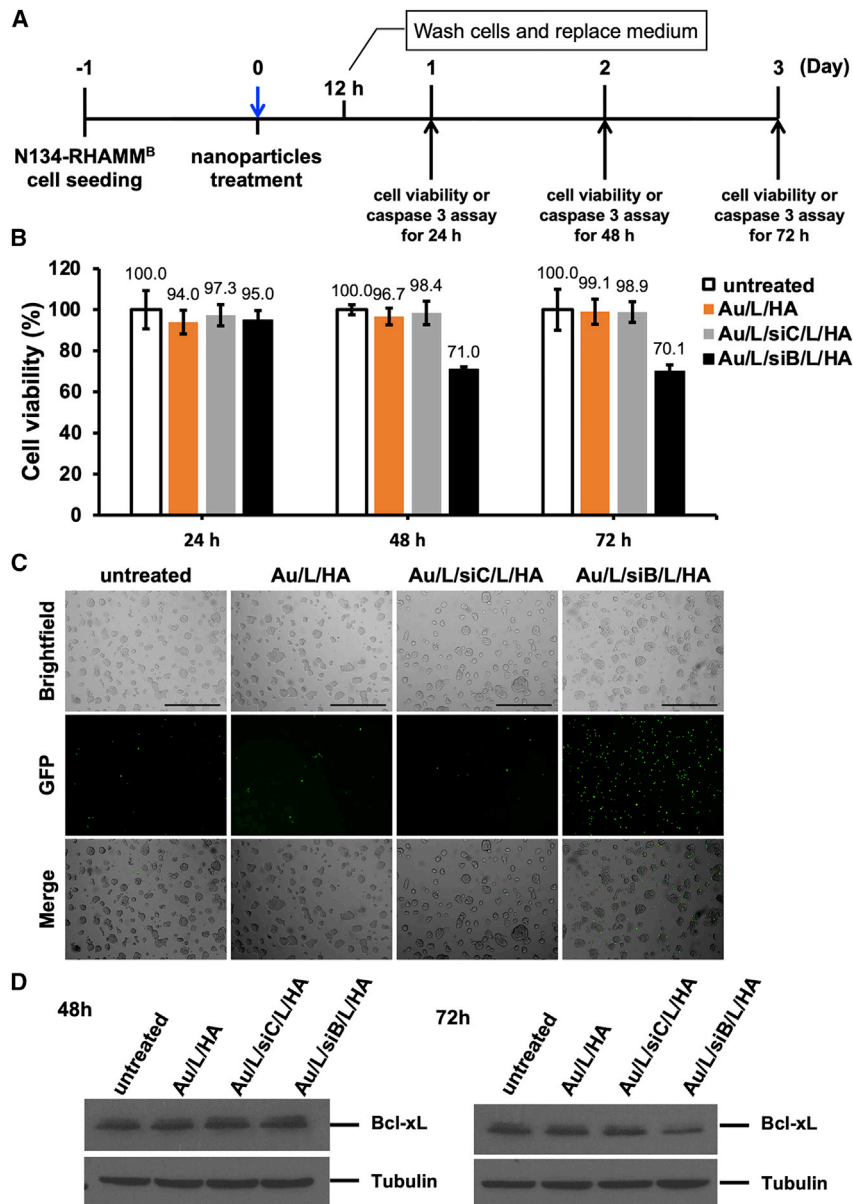
Figure 2. The functional efficacy of the HA-coated AuNPs carrying siBcl-xL (Au/L/siB/L/HA)

(A) Schematic representation of the experiment design. (B) Cell viability of N134-RHAMM[B] cells treated with Au/L/siB/L/HA. Untreated cells and Au/L/siC/L/HA, Au/L/HA were used as controls. The cell viability of the untreated N134-RHAMM[B] were set as 100% and data were shown as mean ± SD. (C) Caspase-3 activity based on the cleaved NucView 488 caspase-3 substrate at the 48 h time point. Scale bar, 400 μm. (D) Western blot analysis of Bcl-xL expression levels in untreated, Au/L/HA, Au/L/siC/L/HA, or Au/L/siB/L/HA-treated N134-RHAMM[B] cells. Tubulin was used as a control loading.

tional 2 layers did not affect the internalization of HA-coated NPs by RHAMM[B]-positive cells.

In N134-RHAMM[B] cells, AuNPs carrying with either siBcl-xL or the KLA peptide alone showed only moderate cell toxicity (71% or 66% viable, respectively). In contrast, siBcl-xL and the KLA peptide combined Au/L/siB/K NPs had a significant cell killing effect (31% viable), suggesting the synergistic therapeutic effect from siBcl-xL and the KLA peptide (Figure 4C). Furthermore, RHAMM[B]-targeting co-delivery of siBcl-xL and the KLA peptide (Au/L/siB/K/HA) led to lowest cell viability (20%, Figure 4C).

Au/L/siB/K/HA NPs inhibits tumor growth in a syngeneic mouse model

To investigate the anti-cancer effect of RHAMM[B]-targeting co-delivery of siBcl-xL and KLA peptide (Au/L/siB/K/HA) *in vivo*, we employed a subcutaneous tumor model using syngeneic mice. N134-RHAMM[B] cells were subcutaneously inoculated to *RIP-TVA* syngeneic mice. After tumor burden reaches 4 mm³, the mice were randomly divided into 3 treatment groups (n ≥ 3 per group) (1) untreated, (2) Au/L/HA control NP, and (3) Au/L/siB/K/HA NP. The NPs were injected via tail vein twice weekly for 2 weeks (Figure 5A).

91% of cells remained viable in N134 cells treated with Au/L/siB/K/HA NPs (Figure 4C). On the other hand, both positively charged NPs, including Au/L/siC/L, Au/L/siB/L, Au/K, Au/L/siB/K, and HA-coated negatively charged NP, including Au/L/HA, and Au/L/siB/K/HA were internalized by N134-RHAMM[B] cells (Figure 4B). It indicated that the positively charged particles, which have PLL or KLA as the surface layer, non-specifically entered cells, while the negatively charged particles, which have HA as the surface layer, only entered the N134-RHAMM[B] cells thought RHAMM[B]. The percentages of the cellular uptake between Au/L/HA and Au/L/siB/K/HA in N134-RHAMM[B] cells by cell counting were similar, 96.3% and 95.1%, respectively (Figure 4B; data not shown), suggesting that the addi-

The tumor growth rates were similar between untreated control and Au/L/HA treatment (Figure 5B, GEE method: p = 0.253). On the other hand, the difference in the growth rate between the Au/L/siB/K/HA treated tumors and Au/L/HA treated tumors was significant (Figure 5B). Tumor size in the Au/L/siB/K/HA treated mice decreased 0.059 per day (in log scale) compared to that in the Au/L/HA treated mice (GEE method: p = 0.0001), suggesting that Au/L/siB/K/HA treatment dramatically inhibited tumor growth. After 2 weeks of treatment, mice were euthanized to harvest tumors and major organs. Tumor weight in (3) Au/L/siB/K/HA NP group was significantly lighter (~35%, p < 0.0001) than that in (1) untreated control and (2) Au/L/HA control NP groups (Figure 5C).
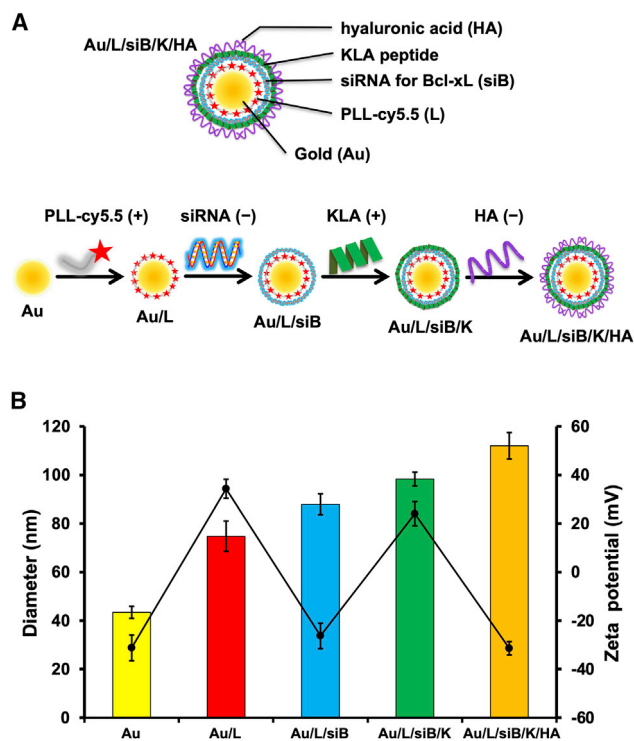
Figure 3. Characterization of the RHAMM[B]-targeting combinational nanocomplex, Au/L/siB/K/HA

(A) Schematic illustrating the process of preparing multilayered Au/L/siB/K/HA by electrostatic interaction. The negatively charged AuNP core was sequentially layered with PLL-Cy5.5 (+), siB (−), KLA-FITC (+), and HA (−) using charge-charge interactions. (B) The average size (color bars) and zeta potential (black line) in the preparation of Au/L/siB/K/HA. Data were shown as mean ± SD. siB, Bcl-xL siRNA; K, KLA peptide; HA, hyaluronic acid.

To trace the biodistribution of the NPs, we have conjugated Cy5.5 with PLL inside the NPs. We measured the Cy5.5 signal of tumors and the major organs via *ex vivo* imaging at the end point (Figure 5D). Only the tumors from the two NP-treated groups presented intense fluorescence of Cy5.5 signal, but not the tumors from the untreated group (Figure 5D, upper middle wells in each 6-well plate), suggesting that intravenously (i.v.) injected HA-coated AuNPs were successfully delivered into RHAMM[B]-positive tumors *in vivo*. While about 4%~9% of Cy5.5 signals were located to the tumors at this time point, the majority of Cy5.5 signals were found in the liver (Figure 5D).

To examine whether the Au/L/siB/K/HA treatment elicited immune responses in the syngeneic mice to suppress tumor growth, the whole tumors were harvested 2 days after the 4th NP treatment and digested into single cells for immune cell profiling by flow cytometry. Cells were stained for surface CD45, CD3, CD8, CD4, B220, MHCII, Ly6G, and Ly6C. We did not observe any significant difference in CD45^{+} cells, CD8^{+} T cells, CD4^{+} T cells, B cells, dendric cells, or myeloid-derived suppressor cells (MDSC) between the Au/L/HA control NP versus Au/L/siB/K/HA group (Figure S5). The data sug-

gested that the suppression of tumor growth by Au/L/siB/K/HA NP treatment was not mediated through host immune responses.

To further evaluate the inhibitory effect of Au/L/siB/K/HA on tumor growth, we analyzed the tumors after 1 week of NP treatment. 5×10^6 N134-RHAMM[B] cells were subcutaneously inoculated to *RIP-TVA* mice. After tumor burden reaches 4 mm³, the mice were randomly divided into 3 treatment groups including (1) untreated, (2) Au/L/HA control NP, and (3) Au/L/siB/K/HA NP. NPs were injected via tail vein twice weekly for 1 week. Similar to the 2-week time point in Figure 5C, tumors in (3) Au/L/siB/K/HA NP group were smaller than that in (1) untreated and (2) Au/L/HA control NP groups (Figure 6A). Histologic analysis revealed that tumors treated with Au/L/siB/K/HA contained more fibrous stroma and were lower in tumor cellularity than untreated and Au/L/HA tumors (Figure 6B). Although scattered cleaved caspase 3-positive apoptotic cells were present in the tumors of (1) untreated and (2) Au/L/HA control NP groups, almost no cleaved caspase-3-positive cells were found in tumors treated with Au/L/siB/K/HA, suggesting a decreased apoptosis and cell turnover in the remaining tumor cells at this stage of stromal fibrosis (Figure 6D). More than 80% of the remaining tumor cells were Ki67-positive in all of these three groups (Figure 6C). Together, these results (Figures 5 and 6) suggested that Au/L/siB/K/HA NP kills tumor cells *in vivo*, and effective tumor inhibition and regression could be expected after multiple cycles of this treatment.

Similar to 2 weeks of NP treatment, we observed the highest accumulation of Cy5.5 fluorescence in the liver via *ex vivo* imaging at this time point (data not shown). We investigated any alteration of histopathological structure of tissues on hematoxylin and eosin (H&E)-stained slides, and observed no damage in the liver, kidney, and other organs (Figures 6E and 6F; data not shown). Taken together, RHAMM[B]-targeting co-delivery of siBcl-xL and KLA peptide (Au/L/siB/K/HA) specifically targeted RHAMM[B]-positive PNET cells and inhibited tumor growth when administrated systemically.

DISCUSSION

Because RHAMM[B] is upregulated in PNETs and many other cancer types, but not expressed in most of normal adult tissues, including the pancreas,[17] we constructed and demonstrated a novel RHAMM[B]-targeting AuNPs co-delivering siBcl-xL and the KLA peptide (Au/L/siB/K/HA) to specifically target RHAMM[B]-positive PNET cells in this study. Systemic administration of this Au/L/siB/K/HA suppressed tumor growth in immunocompetent mice. The elimination of most drugs from the body involves the processes of both metabolism and renal excretion.[30] For many drugs, the principal site of metabolism is the liver, and it is not surprising to see the highest Cy5.5 signal in the liver of the NP-treated animals. Importantly, the Au/L/siB/K/HA did not cause damage in liver, kidney, and other organs.

Although previous studies indicated a possible interaction between CD44 and RHAMM for HA signaling[31,32] and the use of HA-coated NPs to target CD44^{+} cells,[33–35] we found that HA-coated AuNPs
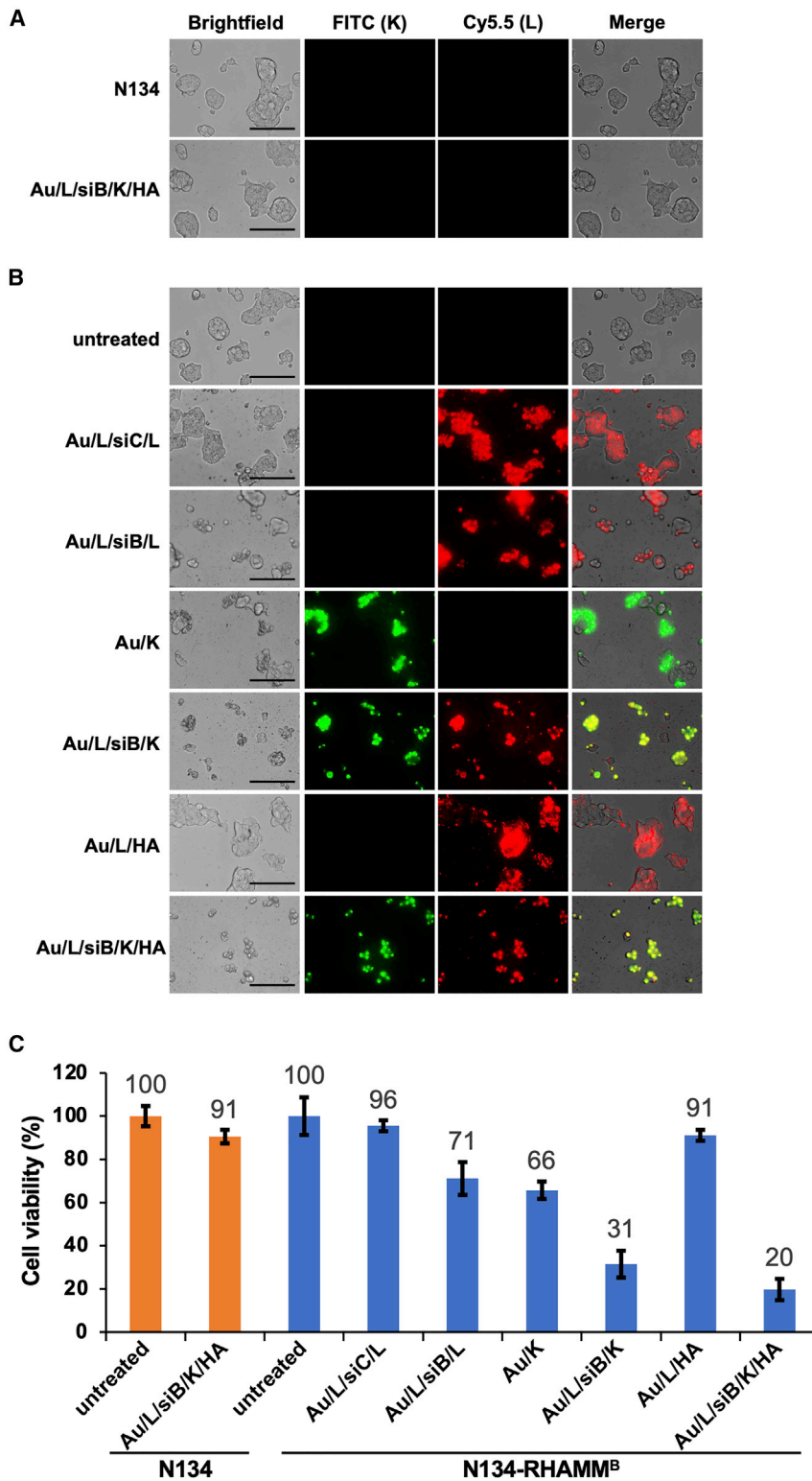
Figure 4. *In vitro* functional efficacy of the RHAMM[B]-targeting combinational nanocomplexes

Images of nanocomplexes uptake in N134 (A) and N134-RHAMM[B] (B) cells (magnification: ×40). Cells were seeded on 96-well plate. After 1 day, cells were treated with Au/L/siB/K/HA or different nanocomplex controls for 12 h and washed twice with PBS. Cells were then incubated in complete medium for additional 48 h. The cellular uptake of NPs was visualized using fluorescence microscopy. Untreated N134 and N134-RHAMM[B] were used as control. Scale bar, 100 μm. (C) Specific synergistic cytotoxic effect induced by the RHAMM[B]-targeting combinational nanocomplex, Au/L/siB/K/HA, in PNET cells. Cell viability of the untreated N134-RHAMM[B] or N134 cells were set as 100% and data were shown as mean ± SD.
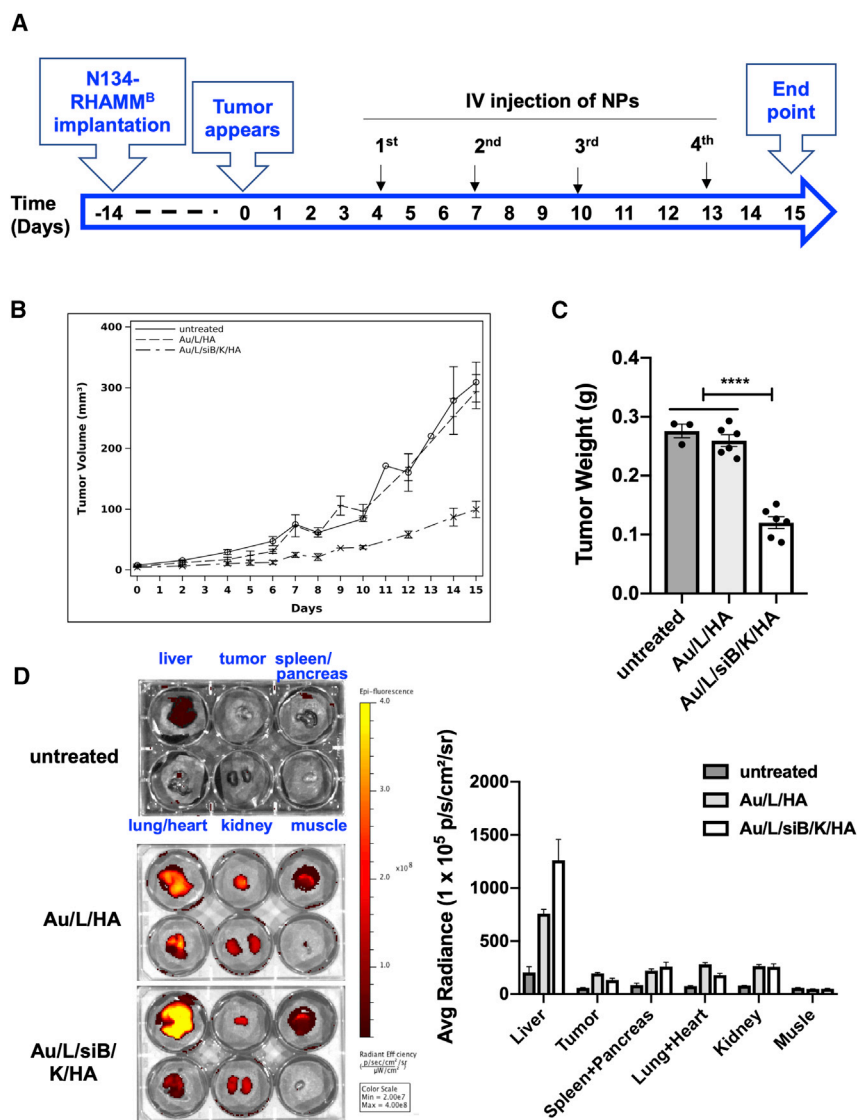
A

B

C

D

Figure 5. *In vivo* therapeutic efficacy and biodistribution of the RHAMM[B]-targeting combinational nanocomplexes

(A) Workflow of *in vivo* study. (B) Tumor size of untreated and Au/L/HA treated control groups versus Au/L/siB/K/HA group. Data were shown as mean ± SEM. (C) Tumor weight of untreated and Au/L/HA treated control groups versus Au/L/siB/K/HA group. Data were shown as mean ± SEM. (D) Analysis of the accumulation of the RHAMM[B]-targeting nanocomplexes in the tumor and major organs. After sacrificing mice, the biodistribution of nanocomplexes was evaluated by optical imaging (IVIS Spectrum) (n ≥ 3 per group). Data were shown as mean ± SEM. ****$p < 0.0001$.

HA on the surface of our AuNPs and in the tumor microenvironment likely have dictated the selective internalization.

We chose AuNP as the core of RHAMM[B]-targeting nanocomplex because it could be made with uniform sizes, good electronic features, and feasibility of surface modification.[37] The use of NPs in delivering siRNA[38] will protect siRNA from nuclease degradation, prolong the circulation time, and improve anti-cancer effect *in vivo*. Our *in vitro* data demonstrated that HA-coated AuNPs carrying siBcl-xL were able to inhibit the expression level of Bcl-xL in N134-RHAMM[B] cells and reduce cell viability. It is intriguing that HA-coated AuNPs carrying siBcl-xL activated caspase-3 activity and induced ∼30% cell death preceding the reduction of Bcl-xL protein levels. None of these events was observed when HA-coated AuNPs carrying scramble control siRNA was used. How siBcl-xL caused apoptosis before executing its knockdown function is fascinating and deserves future studies.

could be successfully internalized by RHAMM[B]-positive mouse PNET cells that had no detectable surface CD44. Therefore, the absence of surface CD44 does not affect the internalization of HA-coated AuNPs by RHAMM[B]-positive PNET cells, and RHAMM[B] expression is sufficient for cellular uptake of the negatively charged HA-coated AuNPs. RHAMM expression peaks at G2/M.[17,36] It is possible that only RHAMM[B]-positive tumor cells in G2/M are susceptible to the NP internalization, and further investigation would be required to determine whether this NP internalization is mediated by a direct interaction between RHAMM[B] and HA-coated AuNPs. Moreover, since HA is already a major component of the extracellular matrix that surrounds migrating and proliferating cells, the mechanism by which HA-coated AuNPs compete with existing HA in the tumor microenvironment for the internalization by RHAMM[B]-positive cancer cells is unknown. We postulate that the different lengths of

This development of RHAMM[B]-targeting combination nanotherapy is of specific clinical interest. We demonstrated that a combination of siBcl-xL and KLA in HA-coated NPs (Au/L/siB/K/HA) offered a synergistic cytotoxic effect. Systemic administration of the Au/L/siB/K/HA significantly suppresses the growth of RHAMM[B]-positive PNET in immunocompetent mice. Since higher RHAMM protein expression is associated with histologically higher-grade tumors in general (e.g., breast, pancreatic, ovarian, endometrial, lung, prostate, colorectal, cervix, esophagus)[17] and Bcl-xL is overexpressed in various cancer types, we expect that this developed strategy could potentially have broad applications for controlling and treating various RHAMM-positive cancers. As Bcl-xL is known to contribute to chemoresistance, we predict that RHAMM[B]-targeting nanotherapy that co-delivers Bcl-xL siRNA and KLA will have a synergistic effect with standard-of-care chemotherapeutics. In addition, RHAMM[B] is an alternative splicing isoform of RHAMM. Its expression is under
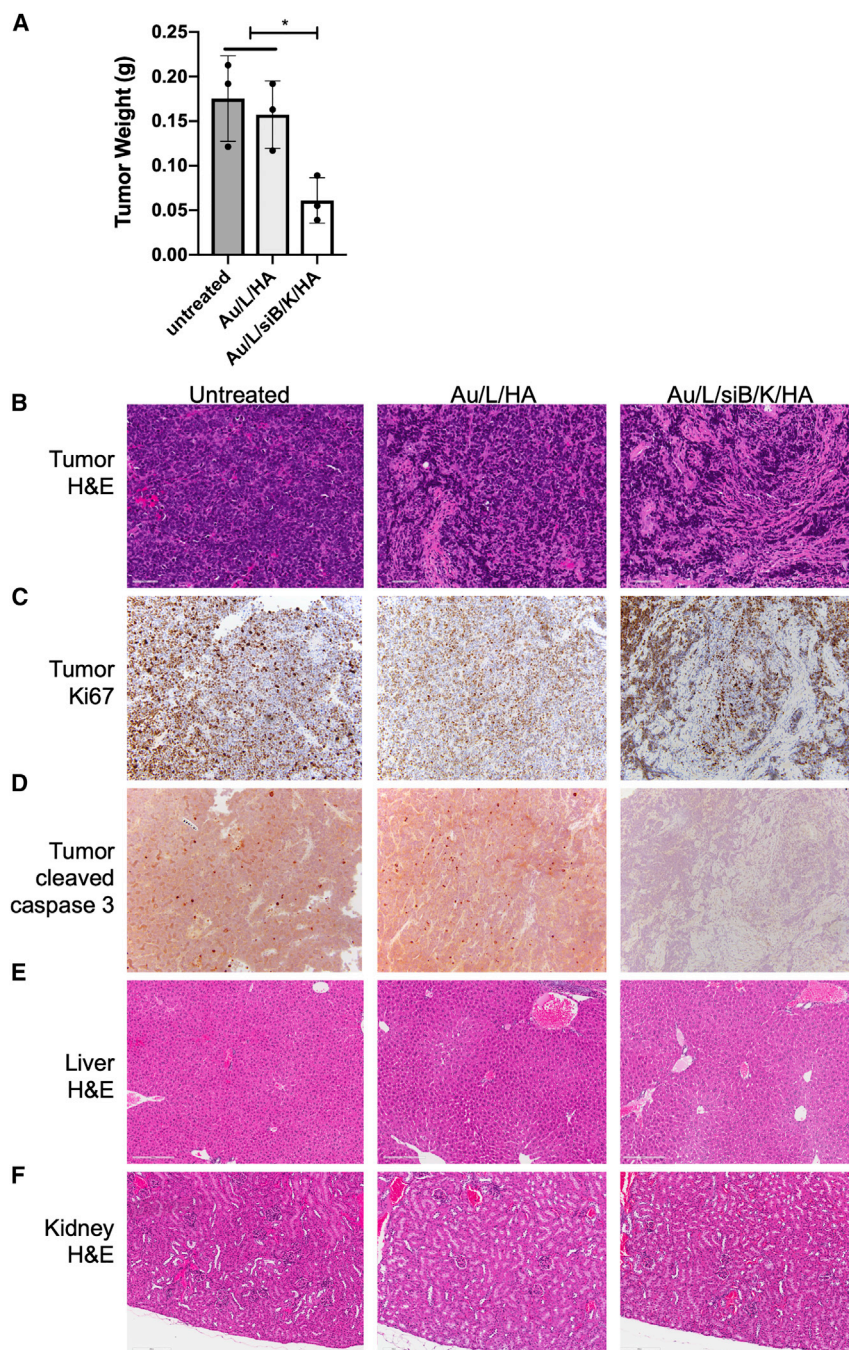
A

Figure 6. Anti-tumor effect and toxicity profile of the RHAMM^B-targeting combinational nanocomplexes

(A) Tumor weight of untreated and Au/L/HA treated groups versus Au/L/siB/K/HA group. N134-RHAMM^B cells were subcutaneously injected into *RIP-TVA* mice. When tumors were visible (4 mm^3), either Au/L/HA (template particles) or Au/L/siB/K/HA (therapeutic particles) were injected via tail vein, twice weekly for 1 week. Mice were euthanized 2 days after final NP treatment. Data were shown as mean ± SEM. H&E of the tumors (B), Ki67 immunohistochemical (IHC) staining of the tumor (C), active caspase-3 IHC staining of the tumors (D), H&E of liver (E), and H&E of kidney (F) after different treatments. Scale bar, 20 μm. *p < 0.05

growth of RHAMM^B-positive PNET. Our technology describes a novel NP-based method and compositions relevant for the treatment of RHAMM-positive cancers. Our systemically injected RHAMM-targeting NPs, which destroy Bcl-xL by siRNA and induce mitochondria fusion by KLA, significantly reduced tumor burden in a pre-clinical mouse model. The RHAMM-targeting NPs carrying siBcl-xL and KLA peptide are anticipated to inhibit many different types of high-grade tumors with minimal adverse effects to healthy cells. The RHAMM-targeting NPs have tunable size, are biocompatible, and have low cytotoxicity. This technology serves a platform to co-delivery of anti-tumor drugs for a synergistic killing effect.

MATERIALS AND METHODS
Chemicals and reagents
Bcl-xL siRNA, PLL (*MW* = 30,000–70,000 g/mol), and diethyl pyrocarbonate (DEPC)-treated water were obtained from Sigma-Aldrich (St. Louis, MO, USA). Bare AuNPs (size: 40 nm) were purchased from BB International (Cardiff, UK), Amersham Cy5.5 Mono NHS Ester was from GE Healthcare (Buckinghamshire, UK), Amicon Ultracel membranes (10 kDa) were from Millipore (Billerica, MA, USA), and sodium HA (*MW* = 100–150 kDa) was from Lifecore Biomedical (Chaska, MN, USA). KLA peptide was synthesized as described.[27]

detection limit in most normal tissues, but it is upregulated in various cancers.[17] If a specific antibody can be identified for this truncated isoform, which lost 15 amino acid residues, RHAMM^B could be a druggable target of antibody-drug conjugate.

In conclusion, we have developed RHAMM^B-targeting combination nanotherapy that carries siBcl-xL and KLA peptide to suppress the

Preparation of PLL-Cy5.5
0.08 mg of Cy5.5 in 100 μL water was mixed with 0.2 mg of PLL in 1 mM 100 μL NaHCO$_3$ in the dark at room temperature for 30 min (vortexed every 10 min) and filtered through molecular-weight cutoff membrane filters (10 kDa, Millipore). The resulting PLL-Cy5.5 was collected and washed several times with sterilized water until the color of the filtrate was clear. The loading ratio of Cy5.5 per PLL was calculated based on the absorbance of Cy5.5 (molar

extinction coefficients = 250,000 m^{-1} cm^{-1} at 678 nm). The Cy5.5/PLL ratio was 4/1.

Preparation of RHAMM-targeting AuNPs

PLL-Cy5.5, Bcl-xL siRNA, amphipathic antimicrobial peptide KLA, and HA were deposited onto the surface of AuNPs (40 nm) using previous modified layer-by-layer fabrication method,[27,39] For a strong layer-to-layer affinity, a previously validated long KLA peptide (28-mer: KLAKLAKKLAKLAKLAKKLAKLAKKLAKLAK) was used in the formulation.[27] The sequences of siRNA against Bcl-xL[40] are sense strand: 5′-GGUAUUGGUGAGUCGGAUCdTdT-3′, antisense strand: 5′-GAUCCGACUCACCAAUACCdTdT-3′, and of scramble control siRNA[40] are sense strand: 5′-UAGGGGUUGCGACGUUUAGdT dT-3′, antisense strand: 5′-CUAAACGUCGCAACCCCUAdTdT-3′. AuNPs (3.15×10^9 particles in 0.7 mL) were added dropwisely onto a PLL-Cy5.5 solution (16.2 nmol in 0.5 mL). After incubating for 30 min in the dark with gentle shaking, the solution was centrifuged for 30 min at $16,100 \times g$ using a micro centrifuge (Eppendorf, Hauppauge, NY). The supernatant was removed, and the gel-like pellet was re-suspended with DEPC-treated water and centrifuged for 30 min at $16,100 \times g$. PLL-Cy5.5-coated AuNPs were stored in DEPC-treated water after additional wash. The next polyelectrolyte layer was attached by adding PLL-Cy5.5-coated AuNPs (in 0.5 mL of pure water) to the Bcl-xL siRNA solution (4.0 nmol, 0.5 mL). The reaction solution was incubated in the dark for 30 min with gentle shaking, followed by three washes. The deposition procedures were repeated sequentially with KLA solution (62.5 nmol, 0.5 mL) and HA solution (8 mg/mL, 0.5 mL) in DEPC-treated water, to have a total of 4 layers of polyelectrolytes (PLL-Cy5.5, Bcl-xL siRNA, KLA, and HA). DLS sizes of each AuNPs were measured using a Malvern Zetasizer (Malvern, Malvern, UK) and zeta potentials using a ZetaPALS (Brookhaven, Holtsville, NY, USA) according to the manufacturer's instructions. The amount of Bcl-xL siRNA and KLA in each nanocomplex was calculated by measuring the concentration of Bcl-xL siRNA or FITC-labeled KLA (KLA-FITC) in the supernatant before and after the coating using a spectrophotometer (Cary 60 UV-Vis, Agilent, Santa Clara, CA, USA). The prepared RHAMM^B-targeting nanocomplexes were stored in DEPC-treated water at 4°C and used within 2 weeks. Other control particles were prepared following the same procedures. Their names and detail compositions were listed in Table 1.

Cell culture and western blot analysis

Generation of N134 cell line has been described.[15,41] RHAMM^B overexpressing cell line, N134-RHAMM^B, was generated using RCASBP as described.[21,42] BON1_TGL_shLacZ and BON1_TGL_shRHAMM cells were generated in the previous study.[18] Cells were cultured in Dulbecco's modified Eagle's medium (DMEM) supplemented with 10% fetal bovine serum (FBS), 2 mM L-glutamine, and penicillin/streptomycin.

For western blot analysis, cell extracts were separated on 10% SDS-PAGE and transferred to nitrocellulose membrane (GE Healthcare). Blots were blocked with 5% (weight/volume) non-fat milk in TBST buffer for 1 h and incubated at 4°C overnight with one of the following primary antibodies at 1:1,000 dilution: RHAMM (Abcam,

ab108339), Bcl-xL (Cell Signaling, #2764), and β-tubulin (Cell Signaling, #2128). The next day, blots were washed with TBST and incubated with secondary antibody (GE Healthcare, #NA934V) at 1:5,000 dilution for 1 h at room temperature. Bands were visualized using ECL Prime Western Blotting System (GE Healthcare).

Live cell imaging of CD44

5,000 cells per well were seeded with 10% FBS-containing DMEM in 96-well flat clear bottom black polystyrene TC-treated microplates (Corning Life Sciences, #3603), and incubated for 48 h. Alexa Fluor 488 conjugated anti-human/mouse CD44 antibody (1:50 dilution, Molecular probes, A25528) was directly added into the cell culture medium of the cells to be stained. After incubation for 30 min at 37°C, the cells were washed with FluoroBrite DMEM (Thermo Fisher, Waltham, MA, USA) and stained with NucBlue Live Cell Stain ReadyProbes reagent (1:50 dilution, Thermo Fisher, R37605) for 15 min at 37°C. Fluorescence images were acquired using a Lionheart FX Automated Microscope with magnification ×20 (BioTek).

Cellular uptake of HA-coated AuNPs

To visualize the cellular uptake, we labeled PLL with a Cy5.5 fluorescent dye. First, cells (N134, N134-RHAMM^B, BON1_TGL_shLacZ, or BON1_TGL_shRHAMM) were seeded on a 96-well black clear-bottom culture plate (Corning Life Sciences, #3603) at a density of 2×10^4 cells per well. After one day, the culture medium was replaced with HA-coated AuNPs (Au/L/HA; 0.08 nmol) containing medium for 12 h. Cells were washed twice with PBS and observed with an EVOS FL Auto Cell Imaging System (Life Technologies, Carlsbad, CA, USA).

Live cell caspase-3 assay

N134-RHAMM^B cells were seeded on μ-Plate 96 Well Black (ibidi GmbH, #89626) at a density of 4×10^4 cells per well. After 24 h incubation, the culture medium was replaced with various nanocomplexes (siControl or siBcl-xL: 0.12 μM) containing medium. After 12 h incubation, cells were washed twice with PBS and further cultured in complete medium. At designated time periods (24 h, 48 h, and 72 h after treatment with each nanocomplexes), cells were replaced with medium containing 5 μM NucView 488 caspase-3 substrate (Biotium, #10403). After 30 min incubation at room temperature, cells were observed directly in medium containing substrate by an EVOS FL Auto Cell Imaging System (Life Technologies) using filter sets for green fluorescence (Ex/Em: 485/515 nm).

In vitro imaging of the RHAMM^B-targeting combinational nanocomplexes

A Cy5.5 fluorochrome and FITC was conjugated with PLL and KLA peptide, respectively, for fluorescence imaging. Briefly, N134 or N134-RHAMM^B cells were seeded on a 96-well black clear-bottom culture plate (Corning Life Sciences, #3603) at a density of 2×10^4 cells per well. After 1 day, the culture medium was replaced with various nanocomplexes (KLA: 1.6 μM, siControl, or siBcl-xL: 0.12 μM) containing medium, and further cultured for 12 h. Cells were then washed twice with PBS, incubated for additional 48 h, and imaged with an EVOS FL Auto Cell Imaging System (Life Technologies).

Cell viability/cytotoxicity assay

N134 or N134-RHAMM[B] cells were seeded on 96-well culture plates at a density of 2×10^4 cells per well. 1 day later, the culture medium was replaced with various nanocomplexes (KLA: 1.6 μM, siControl, or siBcl-xL: 0.12 μM) containing medium. After 12 h incubation, cells were washed twice with PBS. At designated time periods (24 h, 48 h, and 72 h after treatment with each nanocomplex), 10 μL of cell counting kit-8 (CCK-8) solution from CCK-8 (Dojindo Molecular Technologies, CK04) was added to each well and incubated for 3 h. The absorbance of the solution was measured at 450 nm using a plate reader (Tecan, Mannedorf, Switzerland).

Animal studies and histologic analysis

N134-RHAMM[B] cells (5×10^6) were subcutaneously injected into *RIP-TVA* mice (C57BL6 background) on one side of the flank. When tumors reached 4 mm^3, either Au/L/HA (template particles, 150 μL, 10 nmol) or Au/L/siB/K/HA (therapeutic particles, 150 μL; siBcl-xL: 0.67 mg/kg, KLA: 2.84 mg/kg) were injected via tail vein, twice weekly. Mice were euthanized 2 days after final NP treatment. Tumor size was measured using a caliper, and tumor volume (mm^3) was calculated using a standard formula ($W^2 \times L$)/2 × 1000, where L is the long diameter and W is the short diameter. Tumors and main organs were harvested for fluorescence imaging using an IVIS Spectrum imaging system (PerkinElmer, Waltham, MA, USA) with excitation at 640 nm and emission at 700 nm. All procedures involving mice were approved by the Institutional Animal Care and Use Committee. There was no noticeable influence of sex on the results of this study. This study was carried out in strict accordance with the recommendations in the Guide for the Care and Use of Laboratory Animals of the National Institutes of Health. All mice were housed in accordance with institutional guidelines.

For histologic analysis, the excised tumor samples and the organs of interest, including lung, heart, liver, kidneys, spleen, and pancreas, were fixed in 10% formalin overnight and stored in 70% ethanol. Subsequently, tissues and tumors were embedded in paraffin, and 5 μm sections were prepared and stained with H&E Y solution for histologic evaluation via light microscopy. Immunohistochemical (IHC) staining of proliferation index was performed using Ki67 (Abcam, ab16667) antibody on paraffin embedded mouse tissue sections on a Leica Bond system (Buffalo Grove, IL, USA) using the modified protocol F provided by the manufacturer. The section was pre-treated using heat-mediated antigen retrieval with Tris-EDTA buffer (pH = 9, epitope retrieval solution 2) and incubated with the antibody (dilution 1:100) for overnight at room temperature. Signal was detected using an HRP conjugated compact polymer system and DAB as the chromogen. Each section was counterstained with hematoxylin and mounted with Leica Micromount. IHC detection of activated caspase-3, a sensitive and reliable method for detecting and quantifying apoptosis, was similarly performed using cleaved caspase-3 antibody (Cell Signaling, 9664, 1:1,000).

Immune cell profiling

The following antibodies and reagents were used for flow cytometry: CD16/32, CD45-APC (clone 30-F11), CD3-APC/Cy7 (clone 17A2), CD4-PE/Cy7 (clone GK1.5), CD8-PE (clone 53-6.7), B220-FITC (clone RA3-6B2), CD11b-FITC (clone M1/70), Ly6G-PE (clone 1A8), Ly6C-PE/Cy7 (clone HK1.4), CD11c-PE/Cy7 (clone N418), MHCll-APC/Cy7 (clone M5/114.15.2), and Live/Dead Zombie UVTM Fixable viability kit were purchased from BioLegend. All antibodies were tested with their isotype controls. Primary tumor tissues were harvested, weighed, and digested with tissue dissociation buffer (∼280 U/mL Collagenase type III, 4 μg/mL DNase in HBSS) for 1 h in 37°C water bath with periodic vortexing and then mashed through 70 μm filters to get single cell suspension. After 20 min incubation with Zombie UV Fixable stain at room temperature, all samples were washed with BD FACS buffer and stained with the appropriate surface antibodies. Data acquisition was performed on FACSCalibur (BC Biosciences) and analyzed via FlowJo.

Statistical analysis

Each experiment was repeated independently at least three times. Unless otherwise noted, data are presented as mean and SEM. Student's *t* test was used to compare two groups of independent samples. One-way ANOVA was used to test differences among three groups, followed by post hoc comparison with Dunnett test to adjust p values for multiple pairwise comparisons.

To compare the overall difference of tumor growth over time, we transformed tumor size to nature log scale before analysis and used a GEE method to test the significance of difference. All statistical comparisons were two-sided with an alpha level of 0.05 as the significance cutoff. Analyses were performed in statistical software SAS Version 9.4 (SAS Institute, Cary, NC, USA).

SUPPLEMENTAL INFORMATION

Supplemental information can be found online at https://doi.org/10.1016/j.omto.2021.10.002.

AUTHOR CONTRIBUTIONS

X.C., S.K.L., M.S., T.Z., and M.S.H. designed/performed the experiments and analyzed the data. Y.-T.C. contributed immunohistochemical interpretation. Z.C. performed statistical analysis. X.M., C.-H.T., and Y.-C.N.D. designed the experiments and analyzed the data. X.C., S.K.L., and Y.-C.N.D. wrote the manuscript. All authors edited the manuscript.

DECLARATION OF INTERESTS

The authors declare no competing interests.

REFERENCES

1. Franko, J., Feng, W., Yip, L., Genovese, E., and Moser, A.J. (2010). Non-functional neuroendocrine carcinoma of the pancreas: incidence, tumor biology, and outcomes in 2,158 patients. J. Gastrointest. Surg. 14, 541–548.

2. Yao, J.C., Eisner, M.P., Leary, C., Dagohoy, C., Phan, A., Rashid, A., Hassan, M., and Evans, D.B. (2007). Population-based study of islet cell carcinoma. Ann. Surg. Oncol. 14, 3492–3500.

3. Dasari, A., Shen, C., Halperin, D., Zhao, B., Zhou, S., Xu, Y., Shih, T., and Yao, J.C. (2017). Trends in the Incidence, Prevalence, and Survival Outcomes in Patients With Neuroendocrine Tumors in the United States. JAMA Oncol. 3, 1335–1342.

4. Edge, S., Byrd, D.R., Compton, C.C., Fritz, A.G., Greene, F.L., and Trotti, A. (2010). Exocrine and endocrine pancreas. AJCC Cancer Staging Manual, Seventh Edition (Springer), pp. 241–249.

5. Zhang, J., Francois, R., Iyer, R., Seshadri, M., Zajac-Kaye, M., and Hochwald, S.N. (2013). Current understanding of the molecular biology of pancreatic neuroendocrine tumors. J. Natl. Cancer Inst. 105, 1005–1017.

6. Blumenthal, G.M., Cortazar, P., Zhang, J.J., Tang, S., Sridhara, R., Murgo, A., Justice, R., and Pazdur, R. (2012). FDA approval summary: sunitinib for the treatment of progressive well-differentiated locally advanced or metastatic pancreatic neuroendocrine tumors. Oncologist 17, 1108–1113.

7. Hanahan, D., and Weinberg, R.A. (2011). Hallmarks of cancer: the next generation. Cell 144, 646–674.

8. Ellerby, H.M., Arap, W., Ellerby, L.M., Kain, R., Andrusiak, R., Rio, G.D., Krajewski, S., Lombardo, C.R., Rao, R., Ruoslahti, E., et al. (1999). Anti-cancer activity of targeted pro-apoptotic peptides. Nat. Med. 5, 1032–1038.

9. Inoue-Yamauchi, A., Jeng, P.S., Kim, K., Chen, H.C., Han, S., Ganesan, Y.T., Ishizawa, K., Jebiwott, S., Dong, Y., Pietanza, M.C., et al. (2017). Targeting the differential addiction to anti-apoptotic BCL-2 family for cancer therapy. Nat. Commun. 8, 16078.

10. Al-Harbi, S., Choudhary, G.S., Ebron, J.S., Hill, B.T., Vivekanathan, N., Ting, A.H., Radivoyevitch, T., Smith, M.R., Shukla, G.C., and Almasan, A. (2015). miR-377-dependent BCL-xL regulation drives chemotherapeutic resistance in B-cell lymphoid malignancies. Mol. Cancer 14, 185.

11. Ngoi, N.Y.L., Choong, C., Lee, J., Bellot, G., Wong, A.L.A., Goh, B.C., and Pervaiz, S. (2020). Targeting Mitochondrial Apoptosis to Overcome Treatment Resistance in Cancer. Cancers (Basel) 12, 574.

12. Li, J.Y., Li, Y.Y., Jin, W., Yang, Q., Shao, Z.M., and Tian, X.S. (2012). ABT-737 reverses the acquired radioresistance of breast cancer cells by targeting Bcl-2 and Bcl-xL. J. Exp. Clin. Cancer Res. 31, 102.

13. Mason, K.D., Carpinelli, M.R., Fletcher, J.I., Collinge, J.E., Hilton, A.A., Ellis, S., Kelly, P.N., Ekert, P.G., Metcalf, D., Roberts, A.W., et al. (2007). Programmed anuclear cell death delimits platelet life span. Cell 128, 1173–1186.

14. Croce, C.M., and Reed, J.C. (2016). Finally, An Apoptosis-Targeting Therapeutic for Cancer. Cancer Res. 76, 5914–5920.

15. Choi, S., Chen, Z., Tang, L.H., Fang, Y., Shin, S.J., Panarelli, N.C., Chen, Y.T., Li, Y., Jiang, X., and Du, Y.N. (2016). Bcl-xL promotes metastasis independent of its anti-apoptotic activity. Nat. Commun. 7, 10384.

16. Turley, E.A. (1982). Purification of a hyaluronate-binding protein fraction that modifies cell social behavior. Biochem. Biophys. Res. Commun. 108, 1016–1024.

17. Chen, Y.T., Chen, Z., and Du, Y.N. (2018). Immunohistochemical analysis of RHAMM expression in normal and neoplastic human tissues: a cell cycle protein with distinctive expression in mitotic cells and testicular germ cells. Oncotarget 9, 20941–20952.

18. Choi, S., Wang, D., Chen, X., Tang, L.H., Verma, A., Chen, Z., Kim, B.J., Selesner, L., Robzyk, K., Zhang, G., et al. (2019). Function and clinical relevance of RHAMM isoforms in pancreatic tumor progression. Mol. Cancer 18, 92.

19. Schatz-Siemers, N., Chen, Y.T., Chen, Z., Wang, D., Ellenson, L.H., and Du, Y.N. (2020). Expression of the Receptor for Hyaluronic Acid-Mediated Motility (RHAMM) in Endometrial Cancer is Associated With Adverse Histologic Parameters and Tumor Progression. Appl. Immunohistochem. Mol. Morphol. 28, 453–459.

20. Wang, D., Narula, N., Azzopardi, S., Smith, R.S., Nasar, A., Altorki, N.K., Mittal, V., Somwar, R., Stiles, B.M., and Du, Y.N. (2016). Expression of the receptor for hyaluronic acid mediated motility (RHAMM) is associated with poor prognosis and metastasis in non-small cell lung carcinoma. Oncotarget 7, 39957–39969.

21. Du, Y.C., Chou, C.K., Klimstra, D.S., and Varmus, H. (2011). Receptor for hyaluronan-mediated motility isoform B promotes liver metastasis in a mouse model of multistep tumorigenesis and a tail vein assay for metastasis. Proc. Natl. Acad. Sci. USA 108, 16753–16758.

23. Ashraf, S., Pelaz, B., del Pino, P., Carril, M., Escudero, A., Parak, W.J., Soliman, M.G., Zhang, Q., and Carrillo-Carrion, C. (2016). Gold-Based Nanomaterials for Applications in Nanomedicine. Top. Curr. Chem. (Cham) 370, 169–202.

24. Lee, S.K., Han, M.S., and Tung, C.H. (2012). Layered nanoprobe for long-lasting fluorescent cell label. Small 8, 3315–3320.

25. Stern, R. (2009). Hyaluronan in cancer biology 1st (Academic Press/Elsevier).

26. Hiraga, T., Ito, S., and Nakamura, H. (2013). Cancer stem-like cell marker CD44 promotes bone metastases by enhancing tumorigenicity, cell motility, and hyaluronan production. Cancer Res. 73, 4112–4122.

27. Lee, S.K., Law, B., and Tung, C.H. (2017). Versatile Nanodelivery Platform to Maximize siRNA Combination Therapy. Macromol. Biosci. 17, 1600294.

28. Law, B., Quinti, L., Choi, Y., Weissleder, R., and Tung, C.H. (2006). A mitochondrial targeted fusion peptide exhibits remarkable cytotoxicity. Mol. Cancer Ther. 5, 1944–1949.

29. Rasmussen, M.K., Pedersen, J.N., and Marie, R. (2020). Size and surface charge characterization of nanoparticles with a salt gradient. Nat. Commun. 11, 2337.

30. Shargel, L., Wu-Pong, S., and Yu, A.B.C. (2012). Applied Biopharmaceutics & Pharmacokinetics (McGraw-Hill Education).

31. Hamilton, S.R., Fard, S.F., Paiwand, F.F., Tolg, C., Veiseh, M., Wang, C., McCarthy, J.B., Bissell, M.J., Koropatnick, J., and Turley, E.A. (2007). The hyaluronan receptors CD44 and Rhamm (CD168) form complexes with ERK1,2 that sustain high basal motility in breast cancer cells. J. Biol. Chem. 282, 16667–16680.

32. Misra, S., Hascall, V.C., Markwald, R.R., and Ghatak, S. (2015). Interactions between Hyaluronan and Its Receptors (CD44, RHAMM) Regulate the Activities of Inflammation and Cancer. Front. Immunol. 6, 201.

33. Wang, H., Agarwal, P., Zhao, S., Yu, J., Lu, X., and He, X. (2016). Combined cancer therapy with hyaluronan-decorated fullerene-silica multifunctional nanoparticles to target cancer stem-like cells. Biomaterials 97, 62–73.

34. Wang, F., Li, L., Liu, B., Chen, Z., and Li, C. (2017). Hyaluronic acid decorated pluronic P85 solid lipid nanoparticles as a potential carrier to overcome multidrug resistance in cervical and breast cancer. Biomed. Pharmacother. 86, 595–604.

35. Jeannot, V., Gauche, C., Mazzaferro, S., Couvet, M., Vanwonterghem, L., Henry, M., Didier, C., Vollaire, J., Josserand, V., Coll, J.L., et al. (2018). Anti-tumor efficacy of hyaluronan-based nanoparticles for the co-delivery of drugs in lung cancer. J. Control. Release 275, 117–128.

36. Sohr, S., and Engeland, K. (2008). RHAMM is differentially expressed in the cell cycle and downregulated by the tumor suppressor p53. Cell Cycle 7, 3448–3460.

37. Daniel, M.C., and Astruc, D. (2004). Gold nanoparticles: assembly, supramolecular chemistry, quantum-size-related properties, and applications toward biology, catalysis, and nanotechnology. Chem. Rev. 104, 293–346.

38. Peer, D., Karp, J.M., Hong, S., Farokhzad, O.C., Margalit, R., and Langer, R. (2007). Nanocarriers as an emerging platform for cancer therapy. Nat. Nanotechnol. 2, 751–760.

39. Lee, S.K., Law, B., and Tung, C.H. (2020). Multifunctional Nanodelivery Platform for Maximizing Nucleic Acids Combination Therapy. Methods Mol. Biol. 2115, 79–90.

40. Mu, P., Nagahara, S., Makita, N., Tarumi, Y., Kadomatsu, K., and Takei, Y. (2009). Systemic delivery of siRNA specific to tumor mediated by atelocollagen: combined therapy using siRNA targeting Bcl-xL and cisplatin against prostate cancer. Int. J. Cancer 125, 2978–2990.

41. Du, Y.C., Lewis, B.C., Hanahan, D., and Varmus, H. (2007). Assessing tumor progression factors by somatic gene transfer into a mouse model: Bcl-xL promotes islet tumor cell invasion. PLoS Biol. 5, e276.

42. Zhang, G., Chi, Y., and Du, Y.N. (2017). Identification and Characterization of Metastatic Factors by Gene Transfer into the Novel RIP-Tag; RIP-tva Murine Model. J. Vis. Exp. 128, 55890.